Shan Jingxuan (Orcid ID: 0000-0003-0667-6733)
Megarbane André (Orcid ID: 0000-0003-0714-2469)

Genetic predisposition to porto-sinusoidal vascular disorder: a functional genomic-based, multi-generational family study

Jingxuan Shan[1,2], André Megarbane[3,4], Aziz Chouchane[5*], Deepak Karthik[1], Ramzi Temanni[6], Atilio Reyes Romero[7], Huiying Hua[8], Chun Pan[8], Xixi Chen[8], Murugan Subramanian[1], Chadi Saad[9], Hamdi Mbarek[9], Cybel Mehawej[3], Eliane Chouery[3], Sirin W Abuaqel[1], Alexander Dömling[7], Sami Remadi[10], Cesar Yaghi[11], Pu Li[8□] and Lotfi Chouchane[1,2,12□]

[1]Genetic Intelligence Laboratory, Weill Cornell Medicine-Qatar, Qatar Foundation, Doha, Qatar

[2]Department of Genetic Medicine, Weill Cornell Medicine, New York, USA

[3]Department of Human Genetics, Gilbert and Rose-Marie Chagoury School of Medicine, Lebanese American University, Lebanon

[4]Institut Jérôme Lejeune, CRB BioJeL, Paris, France

[5]Faculta di Medicina e Chirurgia, Universita Cattolica del Sacro Cuero, Rome, Italy

[6]Janssen Research and Development, Paris, France

[7]Design Group, Department of Pharmacy, University of Groningen, Groningen, Netherlands

[8]Department of Pediatrics, Ruijin Hospital, Shanghai Jiao Tong University School of Medicine, Shanghai, P.R. China

[9]Genome Programme, Qatar Foundation Research, Development and Innovation, Qatar Foundation, Doha, Qatar.

[10]Cytopath Laboratories, Sousse, Tunisia

This article has been accepted for publication and undergone full peer review but has not been through the copyediting, typesetting, pagination and proofreading process which may lead to differences between this version and the Version of Record. Please cite this article as doi: 10.1002/hep.32735

[11]Department of Gastroenterology, Hotel-Dieu de France Hospital, Faculty of Medicine, Saint Joseph University of Beirut, Beirut, Lebanon

[12]Department of Microbiology and Immunology, Weill Cornell Medicine, New York, USA

[*]The current address: Institute of Pathology, University of Bern, Bern, Switzerland

Keywords: Porto-sinusoidal vascular disorder; Genome sequencing; *FCHSD1*; mTOR; CRISPR/Cas9

Correspondence: Lotfi Chouchane, Weill Cornell Medicine-Qatar, Education City, Qatar Foundation, P.O. Box 24144, Doha, Qatar. Email: loc2008@med.cornell.edu;

Pu Li, Department of Pediatrics, Ruijin Hospital, Shanghai Jiao Tong University School of Medicine, Ruijin Er Rd. 197, 200025, Shanghai, China. Email: leerockygood@yahoo.com

List of Abbreviations

BL, bulge loop

DEG, differentially expressed gene

FCHSD1, FCH And Double SH3 Domains 1

H&E, hematoxylin and eosin

HL, hairpin loop

HSC, hepatic stellate cell

HUVEC, Human umbilical vein endothelial cells

MBL, multi-branched loop

mLST8, MTOR associated protein, LST8 homolog

mTOR, Mechanistic target of rapamycin

NCPH, non-cirrhotic portal hypertension

Nwk, nervous wreck

PHT, portal hypertension

PKLR, Pyruvate Kinase L/R

PPI, protein–protein interaction

PSVD, Porto-sinusoidal vascular disorder

PKLR, Pyruvate Kinase L/R

SP, stacked pair

WT, wildtype

Financial support: This work was supported by the Biomedical Research Program (BMRP) funded by Weill Cornell Medicine-Qatar.

Abstract

Background and aims

Porto-sinusoidal vascular disorder (PSVD) is a group of liver vascular diseases featuring lesions encompassing the portal venules and sinusoids unaccompanied by cirrhosis, irrespective of the presence/absence of portal hypertension. It can occur secondary to coagulation disorders or insult by toxic agents. However, the cause of PSVD remains unknown in most cases. Hereditary cases of PSVD are exceptionally rare, but they are of particular interest and may unveil genetic alterations and molecular mechanisms associated with the disease.

Approach and results

We performed genome sequencing of four patients and two healthy individuals of a large multi-generational Lebanese family with PSVD and identified a heterozygous deleterious variant (c.547C>T, p.R183W) of *FCHSD1*, an uncharacterised gene, in patients. This variant segregated with the disease, and its pattern of inheritance was suggestive of autosomal dominant with variable expressivity. RNA structural modelling of human *FCHSD1* suggests that the C-to-T substitution at position 547, corresponding to *FCHSD1*^{R183W}, may increase both mRNA and protein stability and its interaction with mLST8, a key protein of the mTOR pathway. These predictions were substantiated by biochemical analyses, which showed that *FCHSD1*^{R183W} induced high *FCHSD1* mRNA stability, overexpression of FCHSD1 protein, and an increase in mTORC1 activation. This human *FCHSD1* variant was introduced into mice through CRISPR/Cas9 genome editing. Nine out of the fifteen mice carrying the human *FCHSD1*^{R183W} variant mimicked the phenotype of human PSVD, including splenomegaly and enlarged portal vein.

Conclusions

Aberrant FCHSD1 structure and function leads to mTOR pathway overactivation and may cause PSVD.

Introduction

Porto-sinusoidal vascular disorder (PSVD, also previously described as idiopathic non-cirrhotic portal hypertension, hepatoportal sclerosis, idiopathic portal hypertension, obliterative portal venopathy and incomplete septal cirrhosis) is an under-recognised vascular liver disease of unknown aetiology and is clinically characterised by features of portal hypertension (PHT), which some patients do not exhibit at the time of diagnosis, in the absence of a causative disease such as liver cirrhosis, occlusion of the extrahepatic portal vein/hepatic vein, blood disease, parasitic disease, granulomatous liver disease, or congenital hepatic fibrosis.[1, 2] PSVD showcases a wide spectrum of liver histopathological abnormalities that cause an impairment of blood microcirculation in the liver, including portal and perisinusoidal fibrosis, sinusoidal dilatation, and regenerative changes in hepatocytes.[1, 2] One of the main histopathological features of the disease is the obliteration of the small intrahepatic branches of the portal vein.[3] Although the cause of PSVD remains elusive, several contributing factors have been considered, including immunological and haematological disorders, drug toxicity, and infections.

The disease has a worldwide distribution, but it is more common in developing countries, especially those with lower socioeconomic groups. In 1980, it caused 30-40% of instances of portal hypertension cases in Japan and the Indian subcontinent, but only 5% or less recently.[4, 5] It may account for 3-5 percent of instances of in Western nations, and the patients tend to be older (50-69 years) than those in Japan (40-59 years) and India (30-49 years).[1, 6] However, PSVD is probably underdiagnosed or misdiagnosed, because its clinical presentation closely mimics that of cryptogenic cirrhosis.[5] The lack of pathognomonic clinical and laboratory findings makes histological examination of liver tissue samples critically important to achieve a definite diagnosis of PSVD.[7]

Familial cases of PSVD are exceptionally rare; only twenty-seven multiplex families having PSVD running in their heredity have been reported in the literature.[2–5] The identification of the PSVD-causing genes and their functions may provide tremendous insight into the pathogenesis of the disease and open up new areas of investigation. A definite genetic component of PSVD has not yet been identified; both autosomal dominant and recessive inheritance have been proposed. Recently, several candidate genes for PSVD were suggested by applying exome or whole genome sequencing,[8-11] but no direct evidence or functional studies have been provided to corroborate these findings.

By utilising a multi-faceted and comprehensive approach, this study aimed to identify the genetic alterations responsible for PSVD.

Methods

Study subjects

Members of a large multiplex Lebanese family with PSVD participated in the study. Written informed consent was obtained from each subject included in the study and the study protocol conforms to the ethical guidelines of the 1975 Declaration of Helsinki as reflected in a priori approval by the Saint Joseph University of Beirut's Ethical Committee on Clinical Investigation. The initial clinical diagnosis and liver histology, in all five patients (including the deceased one) with PSVD, were performed at the Hotel-Dieu de France Hospital in Beirut, Lebanon. Further clinical investigation, liver biopsies, and treatment of the surviving four patients were conducted in France at the Hôpital Charles Nicolle, Rouen, and Hôpital Beaujon, Clichy.

Genetic and biochemical analysis

Peripheral blood samples were collected from six members (four patients and two unaffected members), and genomic DNA was extracted using QIAamp DNA Maxi Blood Kits (Qiagen, Hilden, Germany). Whole-genome sequencing was performed using a HiSeq 2500 sequencer (30 × average coverage) at Illumina (San Diego, CA, USA). Paired-end libraries were generated from 1 µg of genomic DNA with the Illumina TruSeq DNA PCR-Free Sample Preparation Kit. Genomic DNA was sheared using the Covaris system (Woburn, MA, USA) and the isolated DNA fragment ends were blunt ended, A-tailed, and ligated using sequencing adaptors with index sequences. Excess adapters and enzymes were removed using AMPure beads (Beckman Coulter Genomics, Danvers, MA, USA). Indexed libraries were size-selected to the 350-bp range with bead-based capture, and the concentration of amplifiable fragments was determined applying qPCR quantifications (relative to sequencing libraries with a known concentration).

Normalised libraries were clustered on a c-BOT machine, and 125-bp paired-end sequencing was performed using a HiSeq 2500 system.

Quality control of the Fastq files was performed using FastQC (v0.7.12) (https://www.bioinformatics.babraham.ac.uk/projects/fastqc/). The reads were then aligned to the reference human genome, build GrCh37, using BWA-MEM aligner: 0.7.12-r1039.[12] GATK haplotype caller was used for variant calling on individual samples. The GATK genotype GVCF option was used for joint calling across individual samples. Variant calling was performed using the recommended best practices in GATK, version 3.7. Joint variant file was further subjected to GATK variant quality score recalibration (VQSR).[13] The annotation of variants was performed by using SNPEFF (version: 4.3r, GRCh37.75 Reference Build) and dbNSFP 3.0.[14] Ingenuity® Variant Analysis (http://ingenuity.com) was used to filter out: i) variants with low call quality (<20), low coverage (<10), failing VQSR filter, and present in low complexity region; ii) variants with allele frequencies more than 1% in public database, including 1000G and ExAC project, were excluded unless established as a pathogenic variant; iii) a de novo dominant inheritance model was selected; and iv) only non-synonymous, frameshift, non-sense, and splice-site variants, which could be potentially deleterious based on functional predictions by SIFT, Polyphen, and Mut Taster, were selected.[15-17] To verify the presence of the *FCHSD1* variant, identified by genome sequencing, Sanger sequencing was carried out on the six samples. Details are provided in **Supplementary Information**.

The liver cell line HepG2 and endothelial cell line HUVEC, both of which express low levels of FCHSD1, were used to assess the functional effect of the FCHSD1 variant. Details of the *FCHSD1* mRNA structure modelling, FCHSD1-mLST8 docking, insertion

of *FCHSD1* in lentiviral vector, and *FCHSD1* expression in human hepatocyte HepG2 cells; western blotting; and immunoprecipitation are provided in **Supplementary Information**.

Fchsd1-R181W knock-in mice

A C57BL/6 mouse model with the R181W variant of the *Fchsd1* gene in mice, corresponding to R183W at the human *FCHSD1* locus, was generated at Cyagen Biosciences, Inc. (Santa Clara, CA, USA). The gRNA (target sequence: TCTGGAGGCTGGTCCGAGAATGG, matches reverse strand) against the mouse *Fchsd1* gene, donor oligo-containing R181W (CGG to TGG) variant sites, and Cas9 mRNA were co-injected into fertilised mouse eggs to generate targeted knock-in offspring. F0 founder animals were identified by PCR followed by sequence analysis (primer sequence and sequencing results are shown in **Supplementary Information**), which were bred with wild type mice to test germline transmission and F1 animal generation. Crossing F1 heterozygotes generated five homozygotes and eight heterozygotes. All F2 mice and two F1 heterozygotes were used to observe the effects of the *mFchsd1* variant, especially the phenotypic and biochemical changes. Formalin-fixed paraffin-embedded tissues were used for evaluation of pathological changes after H&E staining. All mice were housed in the animal facility of Ruijin Hospital (Shanghai Jiao Tong University School of Medicine, Shanghai, P.R. China); the animal care and experimental procedures complied with the guidelines on the care and use of laboratory animals were approved by the Ethical Committee and Animal Experiments at Ruijin Hospital, Shanghai Jiao Tong University School of Medicine. More details on CRISPR/Cas9 genome editing in mice and phenotype assessment are provided in **Fig. S1**.

Statistical Analysis

Statistically analysis was performed using GraphPad Prism 8. Unpaired Student's t tests were performed for comparison of two groups and two-tailed *P* value < 0.05 was considered statistically significant. Two-way ANOVA was performed for comparison of mean difference of two groups and *P* value < 0.05 was considered statistically significant.

Results

Clinical characteristics of the patients

The pedigree of the family with PSVD is shown in **Fig. 1A**. Six members were recruited between Jun 5, 2014, and Nov 12, 2015, and the study was done from May 2, 2017, to Nov 5, 2021. The patterns of inheritance were consistent with autosomal dominant disease with variable expressivity. All affected members fulfilled the clinical and histopathological criteria for PSVD (**Table S1**, **Fig. 1B** and **Fig. S2**). Portal vein thrombosis and Budd–Chiari syndrome were excluded from all affected family members. Further investigations including general metabolites screening were also performed to rule out metabolic diseases. Hepatic viral markers (HBV, HCV and HAV) and autoimmune liver markers were negative.

The proband (IV-2), a 15-year-old boy born to a non-consanguineous Lebanese family. He was born at term after uncomplicated pregnancy, labor, and delivery. Physical examination at birth demonstrated weight, height and circumferences within normal ranges. His past clinical history was unremarkable until the age of 8 years when he was diagnosed with acute lymphoblastic leukaemia which was treated with an intra-familial bone morrow allograft. Subsequently, the patient achieved complete remission. At age 13 years, he presented with recurrent gastroesophageal variceal haemorrhage. Upper gastrointestinal endoscopy revealed grade III oesophageal varices and portal hypertension. Gastroesophageal bleeding was managed with a distal splenorenal shunt. Extensive evaluation (infectious, metabolic, toxic, and haematological) did not reveal a cause for the liver disease. Serum liver function test results were normal. Liver histology showed portal fibrosis, abnormal portal venules, numerous arterial structures, regenerative nodular changes, perisinusoidal fibrosis, and abnormal spacing of the

central venous structures (**Fig. 1B**). Hepatocytes appeared in cell thick cords. No evidence of cirrhosis, inflammatory liver disease, biliary lesions, or steatosis was found. Based on the histological and clinical findings, the patient was diagnosed with PSVD.

The proband's father (III-2), a 52-year-old man, had his first episode of gastroesophageal variceal haemorrhage at the age of 35. Liver ultrasonography showed an enlarged spleen and a normal-sized liver with venous collaterals adjacent to the portal vein, compatible with PHT. No signs of cirrhosis or portal vein thrombosis were observed. Liver histology demonstrated changes consistent with those observed in the PSVD group. A repeat liver histology at the age of 42 years for suspected hepatocellular carcinoma revealed similar findings.

The proband's paternal aunt (III-5) was initially diagnosed with hepatic polyadenomatosis at the age of 36 years and then diagnosed with PSVD at the age of 45 years. Liver histology revealed changes consistent with those observed in the PSVD group.

The proband's father reported that his brother (III-3) was affected by PSVD, but no clinical or histological evidence was provided. The proband's cousin (IV-6) was diagnosed with PSVD at the age of 15 years after presenting clinical and histological changes consistent with PSVD.

The proband's paternal granduncle (II-3) was diagnosed with PSVD whose liver histology revealed a portal tract with angiomatosis, aberrant blood vessels, sinusoidal dilatation, and nodular regenerative hyperplasia. The patient died of portal hypertension complications.

Genome sequencing and the search of candidate genes

With the assumption of an autosomal dominant inheritance model, chosen in accordance with the PSVD segregation pattern in the family, we searched for variants that occurred *de novo* in all four patients but were absent in the two unaffected members. Of the 11 variants identified, none were identified in genes previously reported to be associated with PSVD and only two were predicted to be pathogenic: a nucleotide substitution c.1456C>T, predicted to result in the amino acid substitution p.(Arg486Trp) in *PKLR*, and another nucleotide substitution c.547C>T, predicted to result in the amino acid substitution p.(Arg183Trp) in *FCHSD1* (NM_033449.3) (**Table S2)**. *PKLR* variants caused pyruvate kinase deficiency, an autosomal recessive disease. Since none of our PSVD patients were homozygous for the *PKLR* variant and showed any clinical symptoms related to pyruvate kinase deficiency (OMIM #266200), we retained *FCHSD1* as the unique candidate gene associated with PSVD running in this family. The R183W substitution in FCHSD1 is predicted to be damaging by PolyPhen-2 and deleterious by SIFT. The identified variant c.547C>T in *FCHSD1* (Chr5: 141028553G>A) was absent in over 14,000 genomes of the Qatar Genome Program dataset[18] and rarely found in gnomAD2.1/3.1,[19] with a maximum allele frequency=0.00003563. This finding supports the deleterious effects of this variant, as predicted by computing tools. Sanger sequencing confirmed the *de novo* occurrence of the identified *FCHSD1* variant in all four patients with PSVD but not in two healthy subjects (**Fig. 1C**).

The variant c.541C>T in *FCHSD1* affects its expression

The region of the FCHSD1 protein surrounding amino acid position 183 is highly conserved across species, and arginine at position 183 is absolutely conserved across

mammals (**Fig. S3**), suggesting that it is critical for the individual's biological fitness. FCHSD1 expression was consistently low in liver tissue in the HPA, GTEx, and FANTOM5 datasets (https://www.proteinatlas.org/ENSG00000197948-FCHSD1/tissue). Ectopic expression of the *FCHSD1*^{WT} *and FCHSD1*^{R183W} variants in HepG2 cells and human endothelial HUVEC cells resulted in high expression levels of FCHSD1 in cells transfected with *FCHSD1*^{R183W} compared to those transfected with *FCHSD1*^{WT} (**Fig. 2A**). Treatment with actinomycin D, which inhibits new RNA synthesis, but not the treatment with MG132, which inhibit protein degradation, had different effect on the protein level of FCHSD1 in HepG2 cells transfected with *FCHSD1*^{R183W} compared to those transfected with *FCHSD1*^{WT}, suggesting that the expression difference might be regulated at RNA level (**Fig. 2B**). Treatment of HepG2 cells with antimycin D showed that mRNA of *FCHSD1*^{R183W} were more resistant to the drug treatment than that of *FCHSD1*^{WT} (**Fig. 2C**). Similar results were also observed at both protein and mRNA levels in HUVEC cells (**Fig. S4A and S4B**). The secondary structures in the RNA, decomposed into nearest-neighbour loops, of both *FCHSD1*^{WT} *and FCHSD1*^{R183W} are shown in **Fig. S5**, and the top ten predictions are listed in **Table S3**. A comparison of the secondary structures and hydrogen bond pseudo-knots revealed several differences between *FCHSD1*^{WT} *and FCHSD1*^{R183W}. For instance, owing to the presence of uracil in *FCHSD1*^{R183W}, the stacked pair-2 (SP2) and two hairpin and bulge loops (HL1 and BL2) split into two paired nucleobases (SP2 and SP3), two harpin loops (HL1 and HL2), and one multi-branched loop (MBL2). Similarly, the top-scoring hydrogen bond pseudo-knotted structures displayed structural rearrangements. This is the case of the HL1, which changes into a new structure containing an MBL2, SP2, SP3, HL1, and HL2. Notably, the hydrogen bond interactions between MBL1 and MBL2 involve the rare variant nucleobase - U49. Additionally, the RNA tridimensional structure of the wild type

was morphologically different, with a more elongated shape than that of the rare variant (**Fig. 2D**). In addition, a significant decrease in the solvent-accessible solvent area was observed in the rare variant of *FCHSD1* compared to that in the wild type (17879 Å2 *vs.* 20490 Å2). These data indicate that the rare variant could make the predicted RNA structure less accessible to the solvent and, hence, to regulatory proteins that bind to it.

FCHSD1 is involved in mTOR signalling

To gain insight into the function of FCHSD1, we analysed its binding proteins listed in the protein–protein interaction (PPI) database and expanded our analysis to its well-defined *Drosophila* orthologue, the Nervous Wreck (Nwk). One of the Nwk-interacting proteins is fly Lst8, which is homologous to mammalian mLST8 (an mTOR-associated protein). mLST8 is a key subunit of mTORC1/2 that binds to mTOR directly and increases its kinase activity. Strong preclinical evidence of mTOR inhibitor has been shown for the treatment of portal hypertension.[20, 21] To investigate the possibility of an interaction between human FCHSD1 and mLST8, we performed protein docking experiments. The most populated cluster contained 44 conformations with centre and lowest weighted scores of -965 and -1178, respectively. The proposed docking model showed that the mLST8 subunit in the mTORC1 complex formed the protein–protein interface with FCHSD1 (**Fig. 3A and 3B**). A close-up inspection of this interface revealed a tight network of interactions distributed across the two clusters (**Fig. S6**). The first cluster includes mainly electrostatic interactions, such as Glu-451 with Arg-115, Arg-380 with Asp-160, Arg-357 with Asp-205, and Arg-98 with Glu-374. By contrast, the second cluster displayed hydrogen bond interactions, such as Arg-71 with Pro-167, Gln-164 with Glu-289, Leu-283 with Glu-163, Val-277 with Gln-209, Arg-67 with Pro-212, and Lys-213.

To validate the observations deduced from *in silico* PPI analysis, we immunoprecipitated FCHSD1 in HepG2^{FCHSD1WT} and HepG2^{FCHSD1R183W} cells. Both FCHSD1^{WT} and FCHSD1^{R183W} bound to mLST8. The FCHSD1^{R183W} protein showed strong binding to mLST8 (**Fig. 3C**). In agreement with the structural analysis, Western blotting showed higher levels of FCHSD1 protein in HepG2^{FCHSD1R183W} than in HepG2^{FCHSD1WT}. Overexpression of FCHSD1 correlated with enhanced mTOR phosphorylation (**Fig. 3D**).

FCHSD1 variant knockin mice mimic the phenotype of human PSVD

Ten heterozygous and five homozygous mice containing the human *FCHSD1^{R183W}* variant were obtained using CRISPR/Cas9 genome editing. No spontaneous death was observed in either group of eleven mice (maintained until the age of 24 weeks) or in four mice maintained (until the age of 44 weeks). Compared to the wildtype mice, the genetically engineered mice inclined to have lower body weight at 24 weeks (**Fig. 4A, left; Table S4**). The heterozygotes showed significantly lower body weight compared to the wildtype or to the homozygotes (**Fig. 4A, right**). Overall, out of the 15 genetically engineered mice, 9 *FCHSD1^{R183W}* carriers (7 heterozygotes and 2 homozygotes) showed PSVD-like symptoms; 8 mice, sacrificed at the age of 24 weeks, were found to have an enlarged spleen or blood clot on spleen (**Fig. 4B and Fig. S7A**), which are typical features of portal hypertension. Histological analysis of the liver did not reveal any obvious pathological abnormalities (**Fig. S8**); however, we observed an overexpression of the Fchsd1 protein and an increase in p70 S6 kinase phosphorylation, which indicates the activation of mTOR in the spleen cells of these mice (**Fig. S7B**). Another carrier of the *FCHSD1^{R183W}* variant (mouse 14, **Table S4**), showed phenotypic abnormalities including lethargy and low body weight. When sacrificed at 44 weeks of age,

enlargement of the portal vein was observed and established by histological analysis (**Fig. 4C and 4D**). Noteworthy, this male mouse had significantly lower body weight compared to the other mice (**Table S4**). An increased Fchsd1 protein level and phosphorylation of mTOR and p70 S6 kinase were noticed in its liver and spleen cells (**Fig. S7C**). Next, regardless of the presence of liver cirrhosis, we examined the expression of molecular markers of pathological alterations associated with PHT in liver tissues. Only endothelial activation markers significantly increased or tended to increase in the R181W variant carriers; in contrast, inflammation, angiogenesis, fibrogenesis, and necroinflammation markers did not significantly increase in these animals (**Fig. S9**). We carried out RNA sequencing and examined differentially expressed genes in liver specimens from wild-type mice and R181W variant carriers to assess the impact of this variant on gene expression (**Table S5, Fig. S10A and S10B**). The metabolic pathways such as steroid hormone production, retinol metabolism, and Xenobiotics biodegradation are prominent in the differentially expressed genes (DEGs) (**Fig. S10C and S10D**). The maintenance of the liver's primary functions, including as metabolism, detoxification, and vitamin storage, involves each of these pathways. The liver transcriptome results strongly suggest that this variant has a pathogenic role in liver disease.

Discussion

Our study revealed the structure and function of *FCHSD1*, a novel and uncharacterised gene, associated with the inheritance of PSVD in a large multi-generational family.

In agreement with previous reports,[8, 22] the *FCHSD1*^{R183W} variant identified in this family segregated with PSVD in an autosomal dominant pattern. Interestingly, the affected members expressed different PSVD symptoms, thus reflecting the variable expressivity of the disease within this family. Our findings, hence, strongly imply the gain-of-function mutation of *FCHSD1* as a potential underlying aetiology of PSVD.

Variant analyses are commonly used to support the diagnosis and management of hereditary diseases. More often, the assessment of variant effects involves the dysfunction of the gene product; however, the disease-causing variants may also affect protein expression through mRNA instability. RNA secondary structures regulate elongation, termination, and translation initiation in both eukaryotic and prokaryotic cells. Thus, mutations in highly conserved regions may have deleterious effects on these biological functions. For example, the substitution of adenine to guanine in CAGUGU, a highly conserved motif in the 5′-UTR of the ferritin light chain results in hereditary hyperferritinemia-cataract syndrome.[23] This mutation prevents the formation of a crucial harpin which ensures the recognition and interaction between the RNA and the iron-responsive element-binding protein at low iron concentrations.[23] Similarly, our *in silico* *FCHSD1*_RNA structure analyses showed that the *FCHSD1*^{R183W} variant causes a change in both the secondary and tridimensional structures of *FCHSD1*_RNA. Consequently, the mRNA folding may be altered, leading to an increase in its thermodynamic stability and eventually in its protein overproduction. Altered mRNA stability has been strongly implicated in the manifestation of various human diseases.[24,

[25] In addition to mRNA stability, its translation represents another fundamental regulation for gene expression. Recent studies have underscored the role of tRNA variation in mRNA degradation.[26] The strong binding found between FCHSD1^{R183W} protein and the mTOR-associated protein, mLST8, could be explained by the loss of the positive charge on the side chain of arginine in FCHSD1^{R183W}, resulting in the release of FCHSD1 from being anchored to the negatively charged phospholipid membrane, which may make FCHSD1 more accessible to mLST8.

The current treatment for PHT often adopts treatment for common high blood pressure and non-selective beta blockers.[27] However, only a subset of patients exhibited a hemodynamic response,[28] which might be detrimental to some patients. Thus, novel therapies are urgently needed.[29] A characteristic of PSVD is enlargement of lymph vessels,[30] which was observed in a rat model of PHT and was underlain by activated mTOR signalling.[20] Polymorphisms in *CD73* and xanthine oxidase genes, both of which are mTOR pathway genes, determined the risk of NCPH in HIV patients.[31] mTOR blockade achieved superior results in NCPH rats, with a significant decrease in portal pressure and spleen size.[20, 21] Collectively, these findings suggest a critical role of mTOR signalling in the molecular pathogenesis of PSVD. Furthermore, mTOR signalling contributes to the development of experimental pulmonary arterial hypertension.[32] Our crystal structure elucidates mLST8's binding site in close proximity of the kinase catalytic pocket[33] and further reveals an intricate complex of other subunits. The stabilisation of protein–protein complexes follows very precise rules of oligomerisation and is a subject of great interest in drug discovery; however, it remains challenging to achieve. Examples of PPI stabilisers include 14-3-3 and their partners, ubiquitin/E2 enzymes and ARF1/Sec7. The proper formation of these interfaces is driven by both shape and

electrostatic charge complementarity.[34] Similarly, the protein–protein interface, as presented in our proposed docking model, displays a dense network of polar interactions. Consequently, this might stabilise the mLST8 conformation downstream in the complex with mTORC1. Recently, loss-of-function mutation of *FCHSD1* was shown to ameliorate chronic obstructive pulmonary disease in a mouse model.[35] *FCHSD1*^{R183W} is a gain-of-function variant for mTOR signalling, which is consistent with the observation in PHT. Alternatively, steroidal farnesoid X receptor (FXR) agonist was effective in both NCPH and cirrhotic PHT experimental models.[36] FXR is an emerging, highly potential therapeutic target for chronic liver disease. FXR activation has been proposed as a biomarker of mTOR inhibition.[37, 38] These data demonstrate that the mTOR signalling pathway plays a central role in the aetiology of PSVD, and mTOR pathway antagonists could be potent anti-PHT therapeutics.

We only observed 60% (9 of 15) of our CRISPR/Cas9 mice—those showing symptoms of human PSVD until 20 months after birth. The low penetrating variant in mice could be explained by the genetic difference between humans and mice and by the late onset and the incomplete penetrance of this idiopathic disease in humans. FCHSD1 level is barely detectable in human hepatic or endothelial cells; however, *Fchsd1* is considerably expressed in murine hepatic or endothelial cells. Hence, a mouse model of mTOR hyperactivation other than the *mFCHSD1* gene model is warranted to verify the role of mTOR in PSVD.

Lymphoid tissues including lymph node, spleen and bone marrow, displayed high levels of FCHSD1 expression (link: t.ly/oLoR), and infiltrating liver immune cells (vascular endothelial cells and T cells) as well as hepatic stellate cells (HSCs) do express

significant levels of FCHSD1 (link: t.ly/BqA3). The development of PVSD has been linked to the infiltration of immune cells in the liver.[36] Moreover, our liver transcriptomic data demonstrated that immune system genes were differently enriched in R181W carriers. Thus, this variation in FCHSD1 expression may reflect an increase in the infiltration of inflammatory cells in the tissue surrounding porto-sinusoidal venules and further contributes to the progression of PSVD. Dysfunction in lipid metabolism may also play a role in PSVD etiology. Our transcriptomic analysis, showing that the top enriched DEGs are involved in lipid metabolism, is consistent with the reported results of a transcriptomic study of a human PSVD cohort.[39] In addition, retinol metabolism is another enriched KEGG pathway in our transcriptomic data. HSCs, which are found in the perisinusoidal region, have the capacity to store vitamin A and control sinusoidal circulation. Vitamin A levels have been associated with PVSD, regardless of the presence of cirrhosis.[40,41] Therefore, it is possible that this FCHSD1 mutation causes HSCs to have a dysfunctional vitamin A metabolism, which contributes to the progression of PSVD.

In summary, our study provides insights into the mechanism mediating the development of PSVD and support the use of mTOR inhibitors as a potential PSVD treatment. Furthermore, our animal model suggests a long disease course in the PSVD genetic model and motivates further studies to identify the environmental factors that influence PSVD progression.

Conflict of interests

All the authors declare no competing interests.

Authors' contributions: LC and JS conceived and designed the study. JS, PL, AC, SWA, and MS performed the biochemical analyses. DK, RT, CS, and HM processed the whole-genome data. PL, HH, CP and XC performed analyses on the mouse model. AM, CY, CM, and EC recruited the family and accessed and verified the clinical data. AC and SR reviewed the histopathology reports. ARR and AD performed the structure prediction and docking analyses. LC wrote the first draft of the manuscript with contributions from all authors. LC, JS, AC, and AM performed a literature search and interpreted the data. LC supervised and coordinated this study. The corresponding author had full access to all data in the study and had final responsibility for the decision to submit for publication.

Data availability

All the variants reported here have been submitted to LOVD website (https://www.lovd.nl). All the RNA sequencing data have been deposited to NCBI Gene Expression Omnibus.

Acknowledgements

We are grateful to the family members who contributed to this study which was supported by the Biomedical Research Program at Weill Cornell Medicine-Qatar.

References

1. Schouten JN, Garcia-Pagan JC, Valla DC, Janssen HL. Idiopathic noncirrhotic portal hypertension. Hepatology. 2011;54:1071–81.
2. De Gottardi A, Sempoux C, Berzigotti A. Porto-sinusoidal vascular disorder. J Hepatol. 2022;S0168-8278(22)00355-5.
3. Franchi-Abella S, Fabre M, Mselati E, et al. Obliterative portal venopathy: a study of 48 children. J Pediatr. 2014;165:190–193.e2.
4. Kmeid M, Liu X, Ballentine S, Lee H. Idiopathic non-cirrhotic portal hypertension and porto-sinusoidal vascular disease: review of current data. Gastroenterology Research. 2021;14:49.
5. Riggio O, Gioia S, Pentassuglio I, Nicoletti V, Valente M, d'Amati G. Idiopathic noncirrhotic portal hypertension: current perspectives. Hepat Med. 2016;8:81–8.
6. De Gottardi A, Rautou P-E, Schouten J, et al. Porto-sinusoidal vascular disease: proposal and description of a novel entity. Lancet Gastroenterol Hepatol. 2019;4:399-411.
7. European Association for the Study of the Liver. EASL Clinical Practice Guidelines: vascular diseases of the liver. J Hepatol. 2016;64:179-202.
8. Koot BG, Alders M, Verheij J, Beuers U, Cobben JM. A de novo mutation in KCNN3 associated with autosomal dominant idiopathic non-cirrhotic portal hypertension. J Hepatol. 2016;64:974–7.
9. Vilarinho S, Sari S, Yilmaz G, et al. Recurrent recessive mutation in deoxyguanosine kinase causes idiopathic noncirrhotic portal hypertension. Hepatology. 2016;63:1977-86.

10. Besmond C, Valla D, Hubert L, et al. Mutations in the novel gene FOPV are associated with familial autosomal dominant and non-familial obliterative portal venopathy. Liver International. 2018;38:358-364.
11. **Wu Y**, **Wu Y**, Liu K, et al. Identification of genetic predisposition in noncirrhotic portal hypertension patients with multiple renal cysts by integrated analysis of whole-genome and single-cell RNA sequencing. Front Genet. 2021;12:775470.
12. Li H, Durbin R. Fast and accurate short read alignment with Burrows–Wheeler transform. Bioinformatics. 2009;25:1754-60.
13. DePristo MA, Banks E, Poplin R, et al. A framework for variation discovery and genotyping using next-generation DNA sequencing data. Nat Genet. 2011;43:491-8.
14. Cingolani P, Platts A, Wang LL, et al. A program for annotating and predicting the effects of single nucleotide polymorphisms, SnpEff: SNPs in the genome of Drosophila melanogaster strain w1118; iso-2; iso-3. Fly. 2012;6:80-92.
15. Adzhubei IA, Schmidt S, Peshkin L, et al. A method and server for predicting damaging missense mutations. Nat Methods. 2010;7:248-9.
16. Kumar P, Henikoff S, Ng PC. Predicting the effects of coding non-synonymous variants on protein function using the SIFT algorithm. Nat Protoc. 2009;4:1073-81.
17. Kircher M, Witten DM, Jain P, O'roak BJ, Cooper GM, Shendure J. A general framework for estimating the relative pathogenicity of human genetic variants. Nat Genet. 2014;46:310–5.
18. Mbarek H, Devadoss Gandhi G, Selvaraj S, et al. Qatar Genome Program Research Consortium. Qatar genome: Insights on genomics from the Middle East. Hum Mutat. 2022;43:499-510.
19. Karczewski KJ, Francioli LC, Tiao G, et al. The mutational constraint spectrum quantified from variation in 141,456 humans. Nature. 2020;581:434–43.

20. Mejias M, Garcia-Pras E, Gallego J, Mendez R, Bosch J, Fernandez M. Relevance of the mTOR signaling pathway in the pathophysiology of splenomegaly in rats with chronic portal hypertension. J Hepatol. 2010;52:529–39.
21. Fernandez M, Mejias M, Garcia-Pras E, Mendez R, Garcia-Pagan JC, Bosch J. Reversal of portal hypertension and hyperdynamic splanchnic circulation by combined vascular endothelial growth factor and platelet-derived growth factor blockade in rats. Hepatology 2007;46:1208–17.
22. Majumdar A, Delatycki MB, Crowley P, et al. An autosomal dominant form of non-cirrhotic portal hypertension. J Hepatol 2015;63:525–7.
23. Celma Nos F, Hernández G, Ferrer-Cortès X, et al. Hereditary hyperferritinemia cataract syndrome: ferritin L gene and physiopathology behind the disease—report of new cases. Int J Mol SCI. 2021;22:5451.
24. Kimchi-Sarfaty C, Oh JM, Kim IW, et al. A “silent” polymorphism in the MDR1 gene changes substrate specificity. Science, 2007;315:525–8.
25. Nackley AG, Shabalina SA, Tchivileva IE, et al. Human catechol-O-methyltransferase haplotypes modulate protein expression by altering mRNA secondary structure. Science. 2006;314:1930–3.
26. Wu Q, Medina SG, Kushawah G, et al. Translation affects mRNA stability in a codon-dependent manner in human cells. eLife 2019;8:e45396.
27. de Franchis R. Revising consensus in portal hypertension: report of the Baveno V consensus workshop on methodology of diagnosis and therapy in portal hypertension. J Hepatol. 2010;53:762–8.
28. Reiberger T, Ulbrich G, Ferlitsch A, et al. Carvedilol for primary prophylaxis of variceal bleeding in cirrhotic patients with haemodynamic non-response to propranolol. Gut. 2013;62:1634–41.

29. Mandorfer M, Bota S, Schwabl P, et al. Nonselective β blockers increase risk for hepatorenal syndrome and death in patients with cirrhosis and spontaneous bacterial peritonitis. Gastroenterology. 2014; 146: 1680–90.e1.
30. Oikawa H, Masuda T, Sato SI, et al. Changes in lymph vessels and portal veins in the portal tract of patients with idiopathic portal hypertension: a morphometric study. Hepatology 1998; 27: 1607–10.
31. Vispo E, Cevik M, Rockstroh JK, et al. Genetic determinants of idiopathic noncirrhotic portal hypertension in HIV-infected patients. Clin Infect Dis. 2013;56:1117–22.
32. **Tang H**, **Wu K**, **Wang J**, et al. Pathogenic role of mTORC1 and mTORC2 in pulmonary hypertension. JACC Basic Transl Sci. 2018;3:744–62.
33. Yang H, Rudge DG, Koos JD, Vaidialingam B, Yang HJ, Pavletich NP. mTOR kinase structure, mechanism and regulation. Nature. 2013;497:217–23.
34. McCoy AJ, Chandana Epa VC, Colman PM. Electrostatic complementarity at protein/protein interfaces. J Mol Biol. 1997;268:570–84.
35. Kawasaki T, Sugihara F, Fukushima K, et al. Loss of FCHSD1 leads to amelioration of chronic obstructive pulmonary disease. Proc Natl Acad Sci U S A 2021;118:e2019167118.
36. Schwabl P, Hambruch E, Seeland BA, et al. The FXR agonist PX20606 ameliorates portal hypertension by targeting vascular remodelling and sinusoidal dysfunction. J Hepatol. 2017;66:724-33.
37. Jung K, Kim M, So J, Lee SH, Ko S, Shin D. Farnesoid X receptor activation impairs liver progenitor cell–mediated liver regeneration via the PTEN-PI3K-AKT-mTOR axis in zebrafish. Hepatology. 2021;74:397-410.
38. **Huang X**, **Zeng Y**, Wang X, et al. FXR blocks the growth of liver cancer cells through inhibiting mTOR-s6K pathway. Biochem Biophys Res Commun. 2016;474:351–6.

39. **Hernández-Gea V**, **Campreciós G**, Betancourt F, et al. Co-expression gene network analysis reveals novel regulatory pathways involved in porto-sinusoidal vascular disease. J Hepatol. 2021;75:924-934.
40. Simbrunner B, Semmler G, Stadlmann A, et al. Vitamin A levels reflect disease severity and portal hypertension in patients with cirrhosis. Hepatol Int. 2020;14:1093-1103.
41. Sy AM, Kumar SR, Steinberg J, Garcia-Buitrago MT, Benitez LRA. Liver damage due to hypervitaminosis. ACG Case Rep J. 2020;7:e00431.

Figure Legends

Figure 1. Pedigree chart of the family and the proband's liver histopathology analysis. **(**A) Autosomal dominant inheritance pattern of family members with idiopathic noncirrhotic portal hypertension. *, the subjects have their genomic DNA analyzed by whole genome sequencing. **(**B**)** Proband's (IV-2) liver histopathology. I: Masson stain showing septal fibrosis (×200); II: Aberrant vessels in portal tracts (H&E, ×400); III: Reticulin stain showing features of nodular regenerative hyperplasia (×100). **(**C**)** Chromatogram of Sanger sequencing results of chr5: 141,028,548-141,028,559. The red box labels the chromatogram at chr5: 141,028,553.

Figure 2. The effect of C>T mutation on FCHSD1 expression. (A**)** The protein level of FCHSD1 in HepG2 cells (control) and HepG2 cells with overexpressed wildtype FCHSD1 ($FCHSD1^{WT}$) and R183W mutant FCHSD1 ($FCHSD1^{R183W}$). The FCHSD1 protein was revealed by anti-FCHSD1 antibody. **(**B**)** The protein level of FCHSD1 in $FCHSD1^{WT}$ and $FCHSD1^{R183W}$ HepG2 cells with/without overnight treatment of actinomycin D (ActD, 1μM) or MG132 (1μM). **(**C) The mRNA levels of FCHSD1 in $FCHSD1^{WT}$ and $FCHSD1^{R183W}$ HepG2 cells with/without ActD treatment for 6 hours. ***, $P<0.001$; ****, $P<0.0001$. **(**D**)** Predicted morphological differences of the short RNA sequence of wildtype and R183W FCHSD1. The nucleobases are represented as green sticks while the folded single strand as gray transparent surface and orange cartoons. 3' and 5' ends are colored in red. The triplet of nucleobases containing the point mutation is framed in red while the position is indicated with asterisks. A, B and C show the data from representative one of at least two independent experiments. The relative expression (RE) of FCHSD1 to GAPDH is the normalized ratio of integrated density measured by ImageJ.

Figure 3. FCHSD1 binds to mLST8 and activates mTOR signaling. Protein-protein docking analysis shows that mLST8 interacts with mTOR1 and FCHSD1 and form two specific protein – protein interfaces. **(**A**)** Crystal structure of mLST8 (magenta surface) in its conformation activating mTOR1 (green surface, PDB ID:4JSN). Protein - protein interface is represented as yellow surface. **(**B**)** Proposed docking model between FCHSD1 and mLST8 represented in green and magenta surfaces respectively. Yellow residues binding mTOR have the same coloring scheme as in (A). **(**C**)** Co-immunoprecipitation (IP) analysis of mLST8 and FCHSD1^{WT} or FCHSD1^{R183W}. The grey box indicates an unspecific band in all four IP lanes. The relative quantification (RQ) of immunoprecipitated mLST8 to FCHSD1 is the normalized ratio of integrated density measured by ImageJ. **(**D**)** The phosphorylation of mTOR Ser2448 and p70S6 kinase Thr389 in HepG2 (CRTL) and FCHSD1 overexpressed (FCHSD1^{OE}) HepG2 cells. The phosphorylation ratio equals to (phosphor-signal/GAPDH-signal)/(total-signal/GAPDH-signal). C and D show the data from representative one of at least two independent experiments.

Figure 4. The characterization of R181W knock-in mice. (A**)** The body weight comparison between wildtype and R181W knock-in mice at age 24 weeks. Het: heterozygote; Hom: Homozygote. *, P<0.05; **, P<0.01. **(**B**)** Representative images of liver and spleen of R181W knock-in mice and wildtype (WT) mice. **(**C**)** Dissected livers and spleens of wildtype mouse and R181W carrier sacrificed at age of 44 weeks. **(**D**)** H & E staining of liver, portal vein, liver artery and spleen of wildtype mouse and R181W carrier with enlarged portal vein sacrificed at age of 44 weeks.

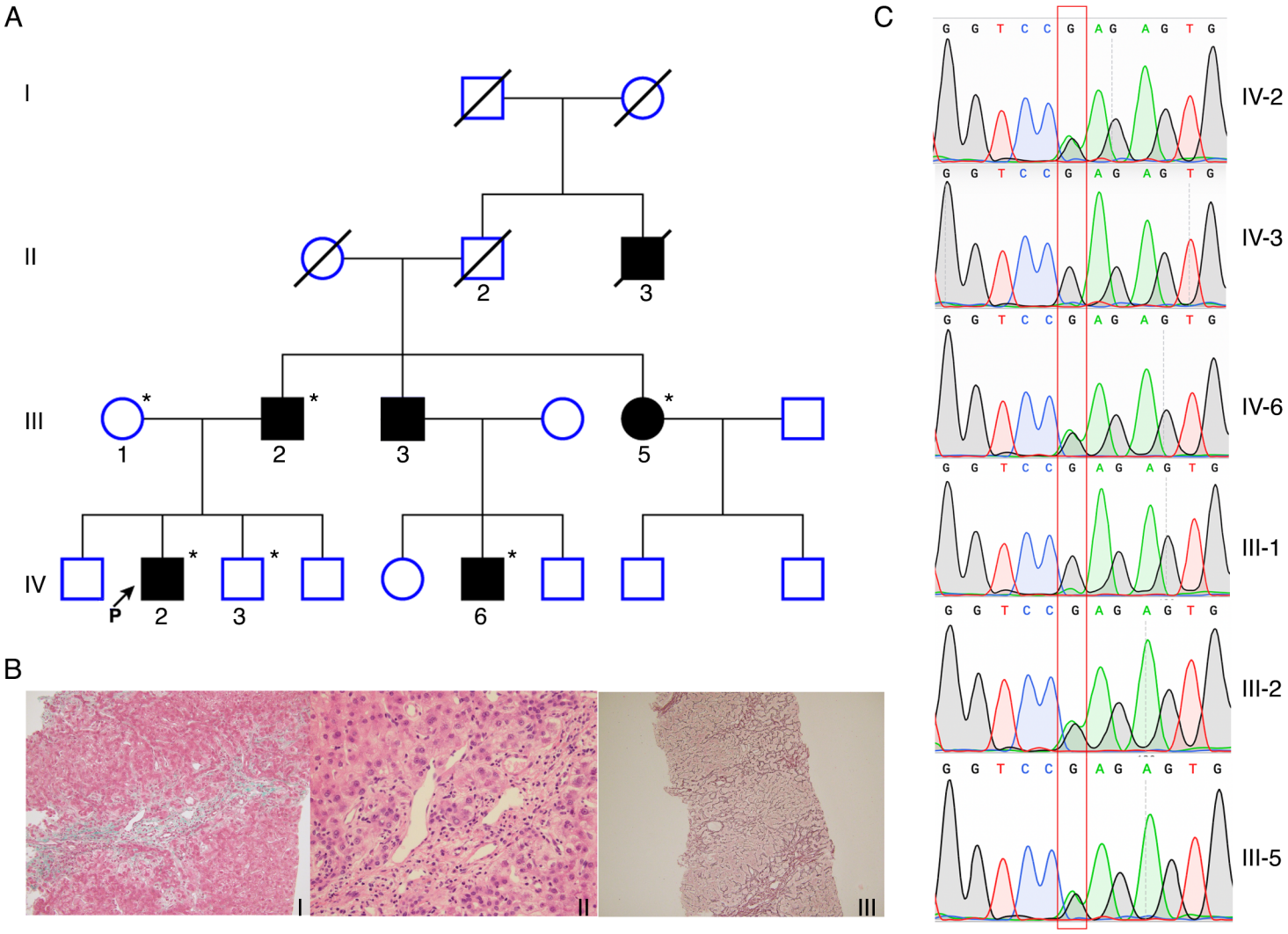

HEP_32735_Figure 1.tif

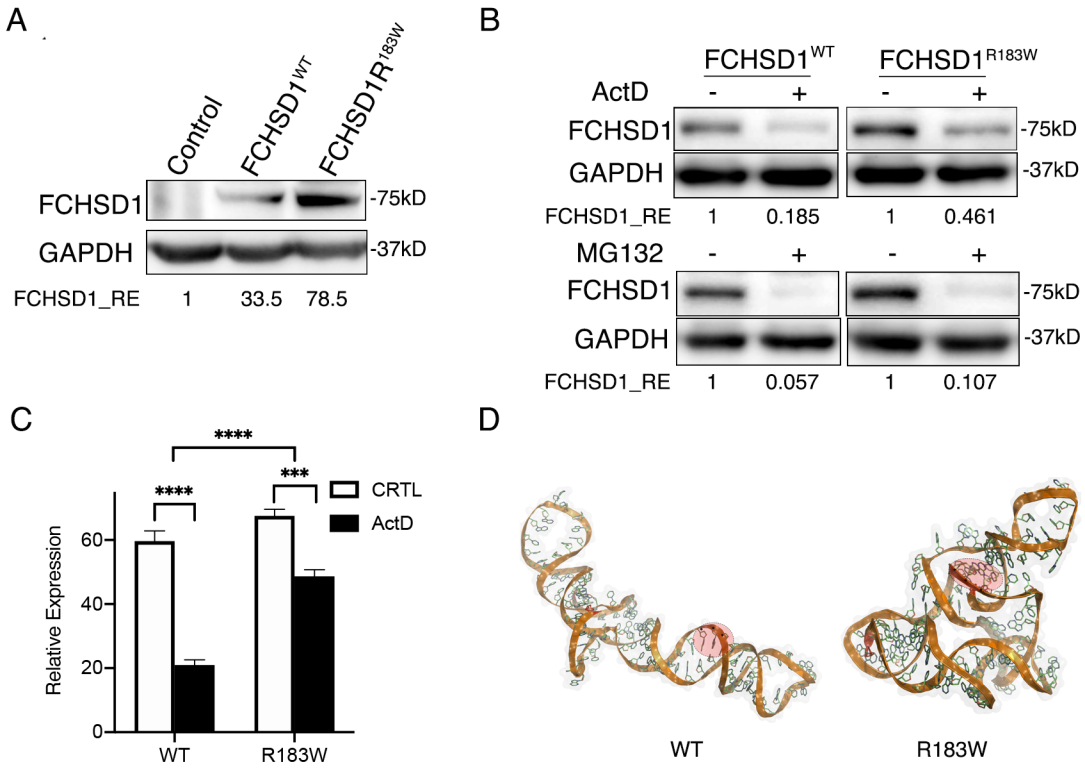

HEP_32735_Figure 2.tif

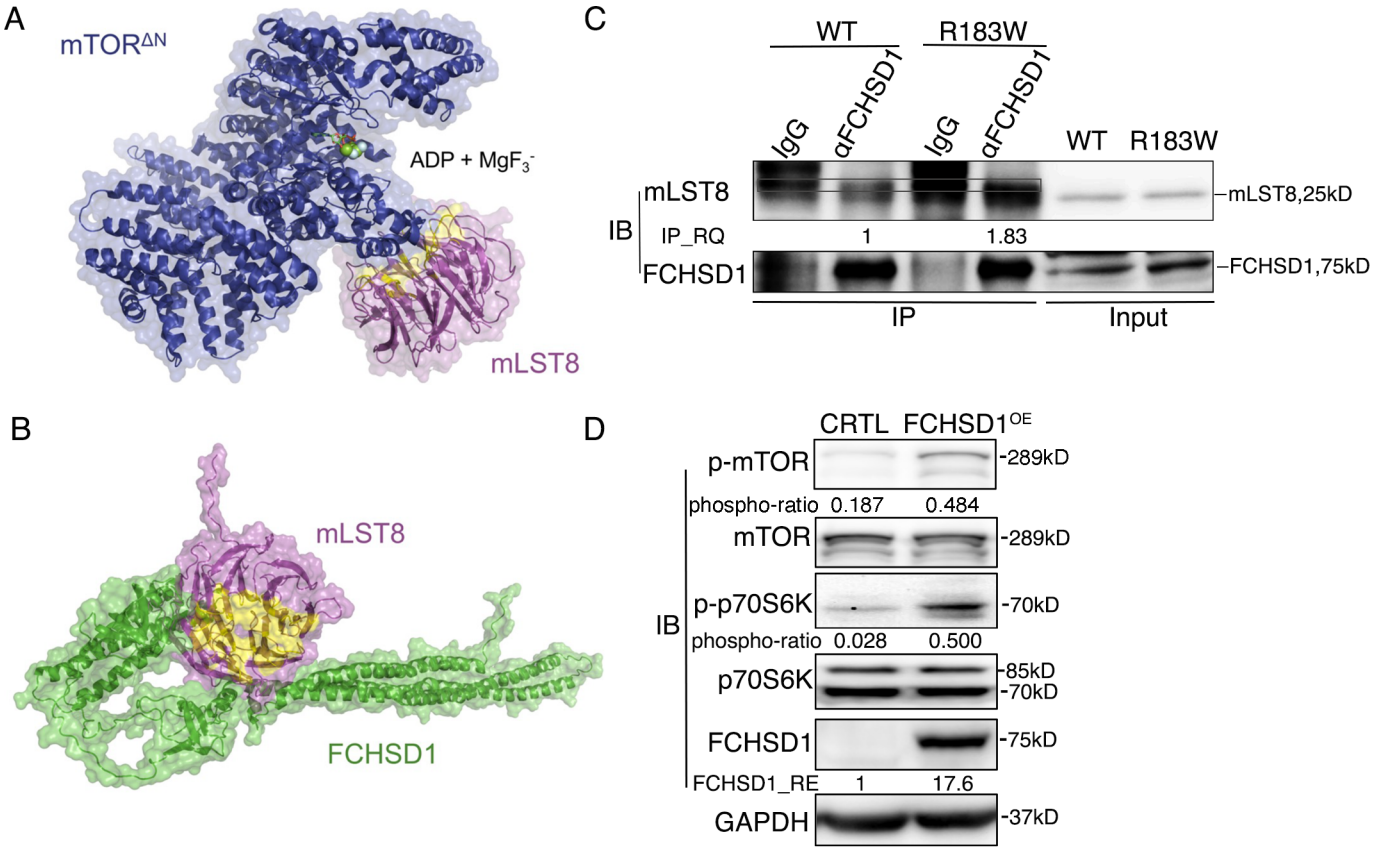

HEP_32735_Figure 3.tif

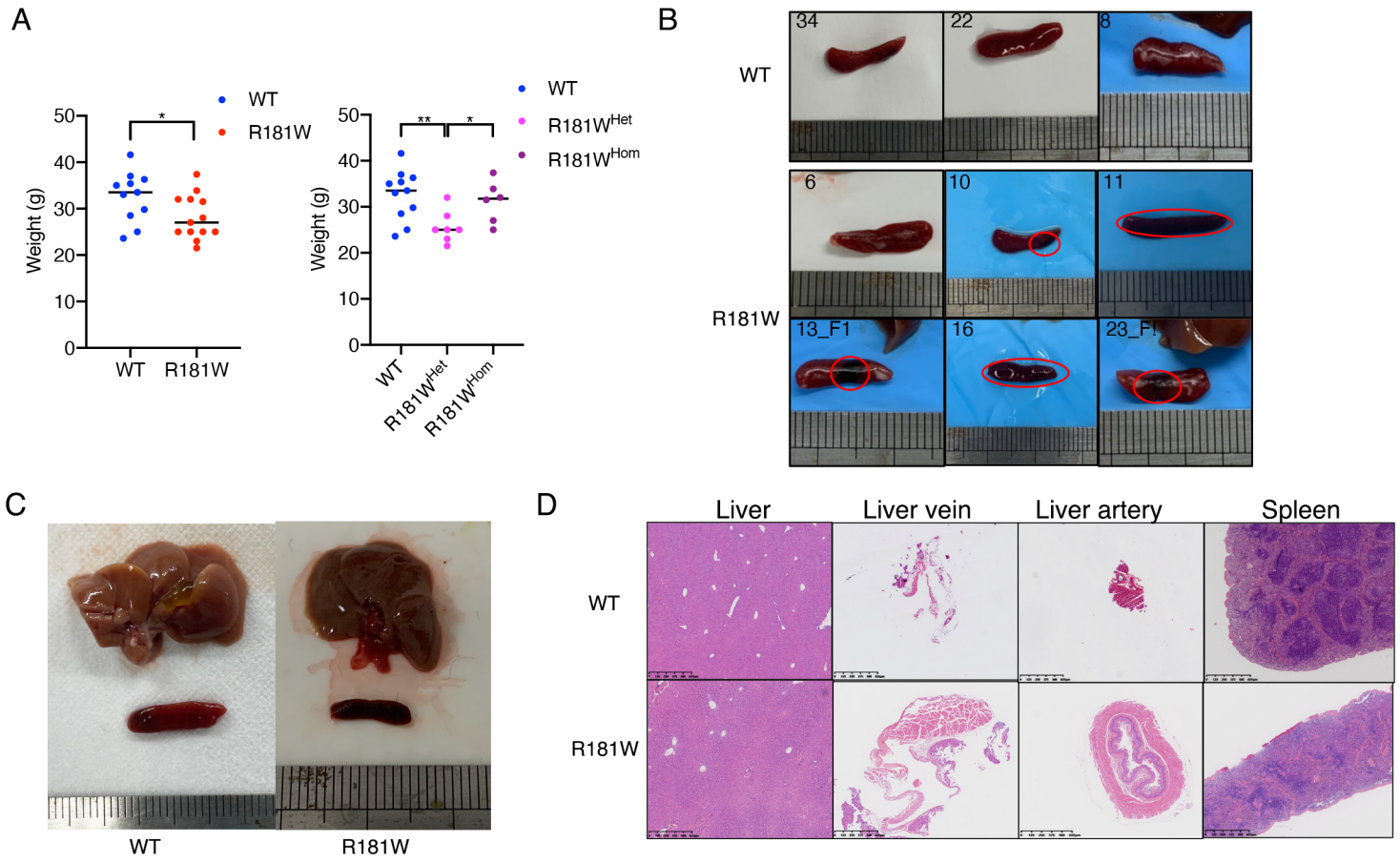

HEP_32735_Figure 4.tif